A&A 496, 453–463 (2009)
DOI: 10.1051/0004-6361/200810671

Astronomy & Astrophysics

Correlation between the spatial distribution of circumstellar disks and massive stars in the young open cluster NGC 6611

II. Cluster members selected with Spitzer/IRAC⋆

M. G. Guarcello[1,2], G. Micela[2], F. Damiani[2], G. Peres[1], L. Prisinzano[2], and S. Sciortino[2]

[1] Dipartimento di Scienze Fisiche ed Astronomiche, Universitá di Palermo, Piazza del Parlamento 1, 90134 Palermo, Italy
e-mail: mguarce@astropa.unipa.it
[2] INAF - Osservatorio Astronomico di Palermo, Piazza del Parlamento 1, 90134 Palermo, Italy

Received 25 July 2008 / Accepted 2 December 2008

ABSTRACT

Context. The observations of the proplyds in the Orion Nebula Cluster, exhibiting clear evidence of ongoing photoevaporation, have provided clear proof of the role of externally induced photoevaporation in the evolution of circumstellar disks. NGC 6611 is an open cluster suitable for study of disk photoevaporation, due to its significant population of massive members and stars with disk. In a previous paper, we obtained evidence of the influence of the strong UV field generated by the massive cluster members on the evolution of disks around low-mass Pre-Main Sequence members. Our study was based on a multiband *BVIJHK* and X-ray catalog compiled for the purpose of selecting cluster members with and without disk.
Aims. We attempt to complete the list of candidate cluster members, using data at longer wavelengths obtained with Spitzer/IRAC, and we reinvestigate the effects of UV radiation on the evolution of disks in NGC 6611.
Methods. In a field of view of $33' \times 34'$ centered on the cluster, we select the candidate members with disks of NGC 6611 using IRAC color–color diagrams and suitable reddening-free color indices. Using the X-ray data to select Class III cluster members, we also estimate disks frequency relative to the intensity of the incident radiation emitted by massive members.
Results. We identify 458 candidate members with circumstellar disks, among which 146 had not been discovered previously. By comparing all color indices used to select cluster members with disk, we claim that these indices measure the excess of radiation due to the emission of the same physical region of the disk (i.e. the inner rim at the dust sublimation radius). Our new results confirm that UV radiation from massive stars affects the evolution of nearby circumstellar disks.

Key words. stars: formation – planetary systems: protoplanetary disks – stars: pre-main sequence – infrared: stars – open clusters and associations: individual: NGC 6611

1. Introduction

Circumstellar disks around young Pre-Main Sequence (PMS) stars have been studied intensely since the discovery of their infrared emission (Mendoza V. 1966, 1968). Until now, several disk models have been developed and a large number of star-forming regions have been observed, in order to understand the physical properties and the evolution of circumstellar disks. Several authors (e.g. Haisch et al. 2001) have claimed that the emission from the inner region of the disks, responsible for NIR excess in T-Tauri stars, declines on a timescale of between ∼1 and ∼10 Myr. Important clues about the typical timescale of disk evolution come from the studies of PMS stars that have cleared the inner region of their circumstellar disks, thus showing excesses in mid- and far-infrared but not in near-infrared bands. These stars with disk are usually considered to be in a transitional phase between Class II and disk-less Class III PMS stars.

The evolution of circumstellar disks can be influenced by nearby massive stars, as demonstrated by observations of evaporating protoplanetary disks in the Trapezium, close to the massive star Θ^1 Ori (see, for example, Störzer & Hollenbach 1999 and references therein). In this case, the photoevaporation process, induced by UV radiation emitted by Θ^1 Ori, dissipates the nearby disks on timescales shorter than 10^6 years. On the other hand, several authors (for example Eisner & Carpenter 2006) have claimed that the externally induced photoevaporation is not an efficient mechanism for the truncation of circumstellar disks around low-mass PMS stars. The debate about this topic remains open.

By comparing the spatial variations in disk frequencies with the positions of massive stars in young open clusters, it is possible to study how the radiation from massive stars affects the evolution of circumstellar disks and the formation of new generations of stars. Balog et al. (2007) and Guarcello et al. (2007), hereafter GPM07, each applied this approach to a young cluster, NGC 2244 and NGC 6611, respectively. In their Spitzer/IRAC-MIPS study of NGC 2244 (at a distance of 1.4−1.7 kpc from the Sun and with an age of about 2−3 Myr), Balog et al. (2007) found that the disk frequency drops dramatically at a distance of 0.5 parsec from the massive cluster members. At larger distances, however, stars with disk do not experience effects induced by massive stars, since the disk frequency is not spatially correlated with their positions.

The young open cluster NGC 6611, in the Eagle Nebula, is also an ideal target for this kind of study, due to its rich PMS population and its large number of massive members (56 with spectral classes earlier than B5; Hillenbrand et al. 1993) distributed

⋆ Optical-infrared catalog of the candidate members of the open cluster NGC 6611 is only available in electronic form at the CDS via anonymous ftp to cdsarc.u-strasbg.fr (130.79.128.5) or via http://cdsweb.u-strasbg.fr/cgi-bin/qcat?J/A+A/496/453

irregularly in the central region of the cluster. To obtain a reliable list of cluster members, GPM07 used a membership criterion based on infrared excesses (to select members with disks) and X-ray emission (to select members without a disk). Due to the high X-ray luminosity of PMS stars, using this criterion it is possible to obtain an unbiased sample of PMS cluster members. With this method, a total of 1122 candidate PMS stars associated with NGC 6611 or the outer part of the Eagle Nebula were identified. In NGC 6611, GPM07 found evidence that the UV radiation from massive stars dissipated the disks around nearby PMS members on short timescales, because the disk frequency declines for small distances from massive members. To obtain this result, GPM07 calculated the flux incident on each cluster members that had been emitted by all the massive stars and then obtained the disk frequency for various bins of incident flux. In this calculation, the projected instead the true distances were used. However, GPM07 demonstrated that this approximation have not effects on their result.

The effects of the energetic radiation from massive stars on the evolution of nearby circumstellar disks have also been studied with simulations of the evolution of open clusters. For example, Adams et al. (2006) claimed that externally induced photoevaporation has no effect on the evolution of disks inside clusters with less than 1000 members. However, more populated clusters, as shown by Fatuzzo & Adams (2008), can host environments in which disks are efficiently evaporated on short timescales, since they have intense UV fields almost independently of the number of stellar members.

This paper represents a follow-up of the GPM07 study, which enriches the list of cluster members by using Spitzer/IRAC data and confirms our main previous results. In a future paper, we will focus on the analysis of the Spectral Energy Distributions of selected cluster members.

The Spitzer/IRAC observations of NGC 6611 used in this work were obtained from the Galactic Legacy Infrared Mid-Plane Survey Extraordinaire (GLIMPSE; Benjamin et al. 2003). The *Infrared Array Camera* (IRAC), mounted on the Spitzer Space Telescope (Fazio et al. 2004), allows the study of stars with circumstellar disks in four infrared bands, centered on 3.6 μm, 4.5 μm, 5.8 μm, and 8.0 μm. In this region of the spectrum, the contribution from the stellar photosphere is usually small compared to the emission from the disk and envelope, and the effects of extinction by the interstellar medium are smaller than at shorter wavelengths. These facts permit a more reliable selection of stars with circumstellar disks than using 2MASS data alone.

Our paper is organized as follows. In Sect. 2, we show the results of the cross-identification between GLIMPSE catalog and the catalog compiled by GPM07. In Sects. 3 and 4, we describe the identification of stars with disks using both IRAC color−color diagram and suitable reddening-free color indices that combine optical and NIR colors. In Sect. 5, we compare the results for the two diagnostics used in this paper. In Sect. 6, we describe the catalog of cluster members. In Sect. 7, we re-examine the results obtained in GPM07 using our updated member list.

2. Multiwavelength catalog

2.1. Description of GPM07 multiband catalog and NGC 6611 parameters

GPM07 compiled a multiband catalog of NGC 6611, using optical observations in *BVI* bands in a 33′ × 34′ field of view centered on the cluster, obtained with the ESO 2.2 m/WFI camera (PI: Mundt), 2MASS public data of the same sky region, and an X-ray observation performed with Chandra/ACIS-I in a 17′ × 17′ region (obs.ID 978; Linsky et al. 2007). Hereafter, we refer to the fields of view of the respective instruments as WFI FOV and ACIS FOV; the latter FOV is contained in the former and is approximately at its center. The catalog compiled in GPM07 consists of 38 995 sources falling inside the WFI FOV.

Using this catalog, GPM07 estimated the age of the PMS members (which are mostly younger than 3 Myr), the distance of the cluster (∼1750 parsec), the anomalous reddening law (with $R_V \sim 3.3$), the average extinction for cluster members ($A_V = 2.6^{\rm m}$), and the relaxation time for the core (4.2 Myr, longer than the age of PMS members). The age of the cluster, however, is not as well constrained as for other cluster parameters. For example, several authors claimed that star formation in this nebula initiated about 6 Myr ago (see Gvaramadze & Bomans 2008, for a detailed discussion about the age spread in this cluster).

In the ACIS FOV, we found 997 X-ray sources using *PWDetect*, a wavelet-based source detection algorithm (Damiani et al. 1997), with 10 expected spurious sources. Among the X-ray sources with optical counterparts, 31 have V magnitudes and $V-I$ colors consistent with foreground main-sequence stars. This fraction of X-ray sources (∼3%) is comparable to the estimated contamination in similar X-ray observations (see, for example, Damiani et al. 2006). However, we will not exclude these sources a priori from our list of candidate cluster members, since they can be Class II YSOs with optical colors altered by effects related to their PMS nature (such as disk gas accretion onto stellar surface). They are instead marked with a special label.

2.2. Cross-identification with GLIMPSE catalog

GLIMPSE observations in the field containing NGC 6611 cover the entire 33′ × 34′ WFI FOV, with the exception of a region towards the North-West of about 7′ × 10′. Following the explanatory manual[1], we selected 41 985 IRAC sources falling in this region.

We identified the sources in common with both the GLIMPSE catalog and the catalog compiled by GPM07 with an identification radius of 0.″3; this value is equal to the astrometric precision of the GLIMPSE catalog relative to 2MASS, as reported in the explanatory manual (in GPM07, we used the 2MASS Point Source Catalog as astrometric reference). In this work, we also include 146 X-ray sources without any optical or 2MASS counterpart, which were not included in GPM07, to identify their possible IRAC counterpart. With the chosen identification radius, we expect about 26 spurious identifications, evaluated with the method defined by Damiani et al. (2006).

The results of the cross-identification are summarized in Table 1. We found 2782 stars with WFI, 2MASS and IRAC detections. This sample exhibits a significant spatial clumping in correspondence to the cluster and it includes 370 X-ray sources, which suggests that it consists mainly of cluster members.

Table 1 also indicates that the 146 X-ray sources without any optical or 2MASS counterpart are not detected even in IRAC observations. Figure 1 shows the spatial distribution of these sources, evidently clustered close to the center of the ACIS FOV. They can be low-mass cluster members with masses lower than the limit of our optical-IR data, since our catalog includes X-ray sources down to the limiting magnitudes of the WFI, 2MASS

[1] Available at http://www.astro.wisc.edu/sirtf/docs.html.

Table 1. Results of the cross-identification.

Number of stars	WFI detection	2MASS detection	IRAC detection	Number of X-ray sources
146	*no*	*no*	*no*	146
20 476	*no*	*no*	*yes*	0
2732	*no*	*yes*	*no*	26
17 768	*no*	*yes*	*yes*	64
12 535	*yes*	*no*	*no*	196
1071	*yes*	*no*	*yes*	178
2648	*yes*	*yes*	*no*	74
2782	*yes*	*yes*	*yes*	370

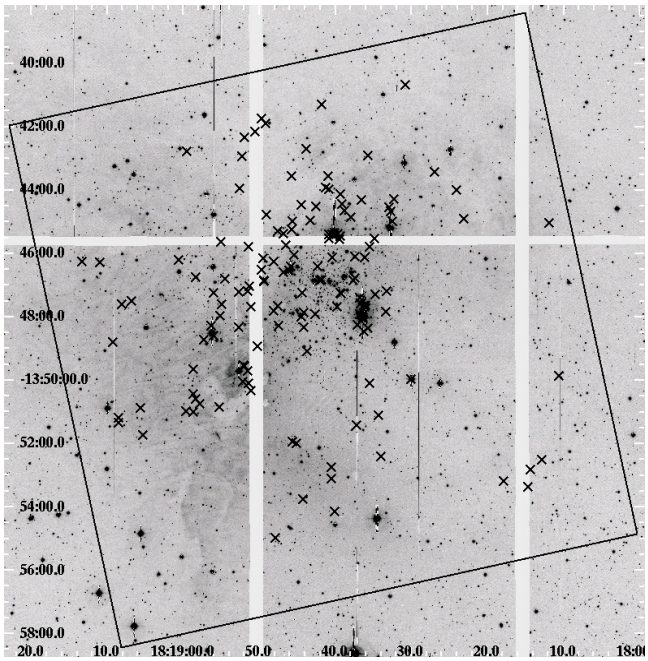

Fig. 1. WFI image, in the I band, of the central region of NGC 6611. Crosses identify the X-ray sources without both optical and infrared counterpart. The box outlines the $17' \times 17'$ ACIS FOV.

and IRAC observations. However, it is also possible that some of these objects are extragalactic sources, detectable in X-rays because the nebula is less dense in correspondence of the cavity cleared by the cluster itself.

GPM07 used detection in ACIS observation as their main membership criterion. This was justified by the fact that almost all our X-ray sources with optical emission are PMS stars compatible with having an age between 0.1 and 3 Myr. Figure 2 shows the V versus $V-I$ diagram for the stars in WFI FOV with errors in V smaller than $0.1^{\rm m}$ and in $V-I$ smaller than $0.15^{\rm m}$. In this diagram, diamonds mark the optical sources detected also at 5.8 μm. About 54% of these objects are bright stars ($V \leq 16^{\rm m}$), while the remaining 46% are fainter and mainly concentrated in the PMS region of the color−magnitude diagram. This region overlaps with that traced by X-ray sources, confirming the youth of these optical-IRAC stars. The V versus $V-I$ diagrams of the sources detected in the other IRAC bands have similar characteristics. Hereafter, the color−magnitude and color−color diagrams of this paper will include only stars with errors in the specific magnitude smaller than $0.1^{\rm m}$ and in color smaller than $0.15^{\rm m}$.

In the next two sections we describe the criteria adopted to select stars with circumstellar disks based on the excesses in their IRAC colors, and we compare them with the criterion based on 2MASS data used by GPM07. These criteria are applied to

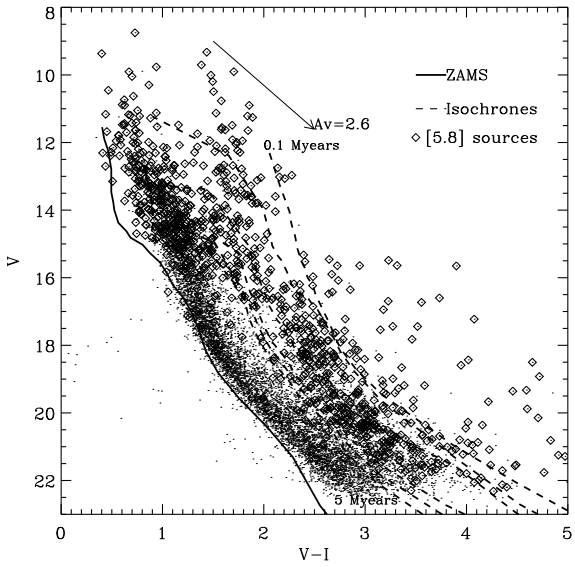

Fig. 2. V vs. $V-I$ diagram of stars in WFI FOV. The thick solid line is the ZAMS (from Siess et al. 2000), at the distance of 1750 pc and with $A_V = 1.45^{\rm m}$ (the average extinction of field stars, evaluated in GPM07). The dashed lines are the isochrones at 0.1, 0.25, 1, 2.5, 3, and 5 Myr, with the average extinction appropriate for cluster members ($A_V = 2.6^{\rm m}$). The extinction vector is obtained from the law of Munari & Carraro (1996). The diamonds are optical sources detected at 5.8 μm.

stars with magnitude errors smaller than $0.1^{\rm m}$; this is a stringent rule when applied to faint stars, since at 3.6 μm more than 50% of stars fainter than $12.5^{\rm m}$ have errors larger than $0.1^{\rm m}$. The same 50% fraction is found at $12^{\rm m}$ at 4.5 μm and at $10.5^{\rm m}$ at both 5.8 μm and 8.0 μm. It is evident, then, that a criterion for the selection of stars with disk using all IRAC bands simultaneously does not allow us to select faint sources with disks, since most of these sources have large errors in their measured magnitudes for IRAC bands at longer wavelength. We partially overcome this problem using two independent disk diagnostics: the usual color−color IRAC diagram (Sect. 3) and a diagnostic based on suitable reddening-free color indices (Sect. 4), involving optical+2MASS photometry and only a subset of IRAC bands.

3. T-Tauri stars from IRAC color–color diagram

The [3.6]−[4.5] versus [5.8]−[8.0] diagram is an excellent tool for identifying stars with circumstellar disks (see, for example, Allen et al. 2004). In this diagram, stars with photospheric colors are clustered around the origin, while stars with disks exhibit colors significantly different from zero. The two populations can be easily distinguished even if the stars are affected by significant interstellar extinctions. This is possible since the reddening vector is almost vertical (due to small effects of reddening in [5.8]−[8.0]) or it is direct toward bluer [5.8]−[8.0] colors (due to the partial overlap of the IRAC 8.0 μm band with the interstellar silicate feature), depending on the adopted extinction law (see, for example, Megeath et al. 2004 and Flaherty et al. 2007). Unlike other possible infrared diagrams, the locus of both reddened photospheres and sources with intrinsic red colors in the IRAC color−color plane are not blended, even for high extinctions.

With this diagram, it is also possible to distinguish roughly embedded Class I and Class II T-Tauri YSOs (Young Stellar Objects): the former have both colors redder than the latter since the presence of the collapsing envelope surrounding the star and

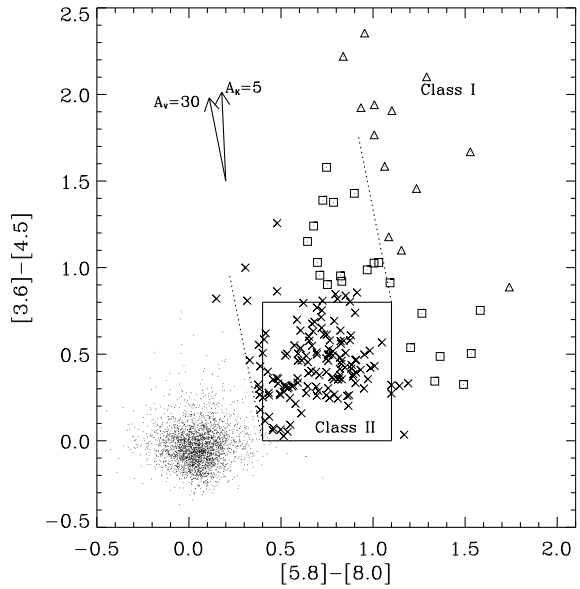

Fig. 3. Color–color diagram for IRAC sources in WFI FOV (dots). The box marks the approximate locus of Class II YSOs (crosses). The dashed lines roughly separate reddened photospheres (*left*), reddened Class II YSOs (*center*), and Class I YSOs (in *the upper right part* of the diagram, marked with triangles). Squares mark stars either classifiable as Class II or Class I YSOs. The reddening vectors with $A_V = 30^m$ and $A_K = 5^m$ are obtained from Megeath et al. (2004) and Flaherty et al. (2007), respectively.

the disk; see, for example, Allen et al. (2004), who used the models developed by D'Alessio et al. (1998, 1999, 2001) for Class II stars and by Kenyon et al. (1993) and Calvet et al. (1994) for embedded Class I stars.

3.1. Classification of selected YSOs

GLIMPSE data of the Eagle Nebula were already analyzed, in combination with 2MASS data, by Indebetouw et al. (2007). We reanalyze the data by using also different methods, for several reasons. First, we note that the selection of stars with a K excess performed by Indebetouw et al. (2007) and GPM07 differed. The latter used the reddening-free color indices, a method far more efficient than the use of the T-Tauri locus (Meyer et al. 1997) in infrared color−color diagrams, that is the method adopted by the former. In GPM07, only stars with color errors ($\sigma_{\rm colors}$) smaller than 0.15^m were used, and we apply the same approach here to be as conservative as possible. With these conditions, we produced a different IRAC color−color diagram from Indebetouw et al. (2007). In the present paper, this diagram is used, together with reddening-free color indices defined with IRAC bands, to perform a selection of the cluster members with disk that is as far as possible model-independent. Furthermore, 2MASS and IRAC data are complemented by optical and X-ray data, which are fundamental in assessing the nature of the candidate members.

Figure 3 shows the color–color diagram for the IRAC sources in WFI FOV used to classify the YSOs. Stars with colors typical of photospheres are clustered around the origin, with a spread consistent with photometric uncertainties and reddening, and clearly separated from sources with intrinsic red colors.

To select and classify stars with a disk, we used the reddening vector obtained by Megeath et al. (2004) from the reddening law of Mathis (1990), shown as the inclined vector in Fig. 3. The question of which extinction law is correct to use in IRAC bands remains unanswered. For this reason, in Fig. 3 we also show the

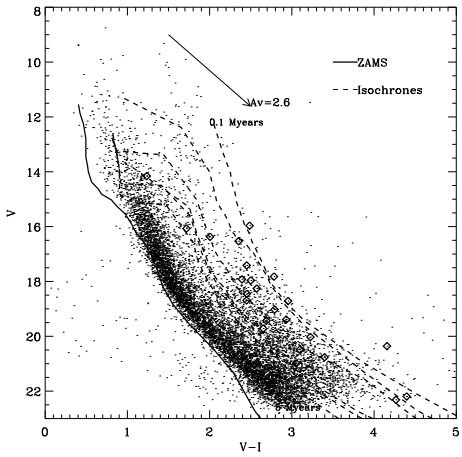

Fig. 4. V vs. $V - I$ diagram analogous to that in Fig. 2. Diamonds mark candidate stars with disks selected by the IRAC color–color diagram but not in GPM07.

extinction vector (the $A_K = 5^m$ arrow) obtained from the mean reddening law recently estimated by Flaherty et al. (2007) in the direction of five nearby star-forming regions. It is evident that the difference between the two extinction laws is relevant only for high extinction.

Using this diagram, we select 147 Class II YSOs as the stars within the box in Fig. 3 (crosses), taking into account photometric uncertainties and extinction. This box was obtained from the models of stars with circumstellar disk developed by D'Alessio et al. (1998, 1999, 2001). In addition, 13 stars are unambiguously classified as Class I YSOs (triangles in Fig. 3).

Twenty-two stars (marked with squares in Fig. 3) are sources with only one IRAC color redder than the Class II locus. Those with $[3.6]-[4.5] \geq 0.8^m$ can be either Class I sources or very embedded Class II YSOs; those with $[5.8]-[8.0] \geq 1.2^m$ are usually interpreted as Class II YSOs, with no emission detected from the inner region of the disk, due to a larger inner hole or to the disk inclination with respect to the line of sight. However, as suggested by Kenyon et al. (1993), Class I YSOs with large centrifugal radii[2] and optically thin envelopes, which exhibit a silicate band in emission, may also have a spectral energy distribution that is consistent with the latter colors. For these reasons, all of these 22 stars can not be clearly classified. The possible contamination by extragalactic sources is discussed in the next section.

The IRAC color–color diagram allows us to select a total of 182 members with excesses, which represents 120 new identifications with respect to GPM07, where *BVIJHK* bands were used. This result is not in disagreement with GPM07, since in that work it was impossible to classify most of these stars. Among these 120 stars, in fact, only 48 have robust measurements in K, 25 in both V and I (shown in Fig. 4) and just 9 in all these three bands simultaneously. We also note that 19 of these stars are also X-ray sources (among the total of 57 that are inside the ACIS FOV), and that the $V-I$ and V values of the subsample with good WFI photometry are consistent with being cluster members.

Figure 5 shows the IRAC colors of 76 X-ray sources with good photometry in the four IRAC bands. A large number of these sources (55) are classified as Class II YSOs while none is classified as Class I sources. This is probably due to lower luminosity in X-rays of Class I objects with respect to more evolved

[2] The distance from the central star at which the infalling material from the envelope with most angular momentum, i.e. close to the equatorial plane, collides with the circumstellar disk.

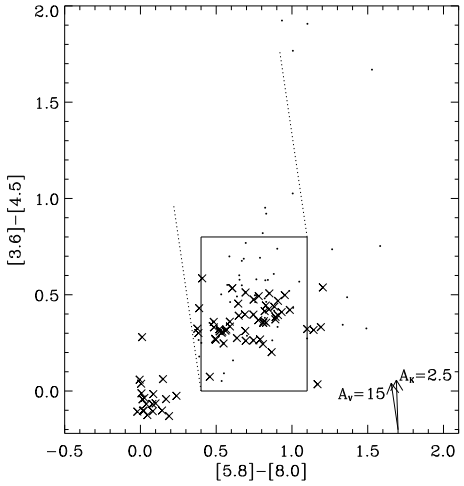

Fig. 5. IRAC color–color diagram of the X-ray sources (crosses). Dots mark the stars with disks selected from the IRAC diagram of Fig. 3, for the sky region contained in the ACIS FOV. The Class II locus and the reddening vectors are analogous to those in Fig. 3.

YSOs, in agreement with that shown by the previous studies of star-forming regions with X-ray observations deeper than our own (i.e. Prisinzano et al. 2008).

3.2. Contaminating sources

To evaluate the contamination due to extragalactic sources, we use the criteria defined in Gutermuth et al. (2008). These criteria allow us to identify candidate AGNs, or galaxies dominated by PAH emission, using various color–color and color−magnitude IRAC diagrams. Using these criteria, we identify only 4 stars that can be extragalactic sources, but their A_V values predicted by the optical colors are too small (between 2.5^m and 5^m) to confirm this classification.

However, in the IRAC color–color plane PAH-rich (Polycyclic Aromatic Hydrocarbons) star-forming galaxies can be found in the locus at $-0.1^m < [3.6]-[4.5] < 0.6^m$ and $[5.8]-[8.0] > 1^m$ (in the part of the diagram redder than the Class II locus). We selected 25 candidate disk-bearing members in this region of the diagram. Some of them could be PAH-rich star-forming galaxies, and we will classify them definitely in a future paper.

3.3. Spatial distribution of Class II and Class I YSOs

Figure 6 shows the IRAC image of the Eagle Nebula at 8.0 μm with the Class II objects (circles) and sources identified to be either Class I or reddened Class II YSOs (crosses) superimposed. In the center of the cluster (approximately in the center of the image) there is a lack of sources of the latter group, with respect to the outer regions. This is not a true result, because it is caused by the intense diffuse emission from the dense structures in the central region of the nebula, like the elephant trunks inside the box in Fig. 6, that complicates the extraction of the IRAC point sources. These structures are heated directly by the radiation from the massive members of NGC 6611, and are extremely bright in the IRAC bands at longer wavelengths. These diffuse structures are also very dense, accounting for an high extinction inside them.

The evidence that star formation activity is still ongoing in the central region of NGC 6611 was provided by several authors.

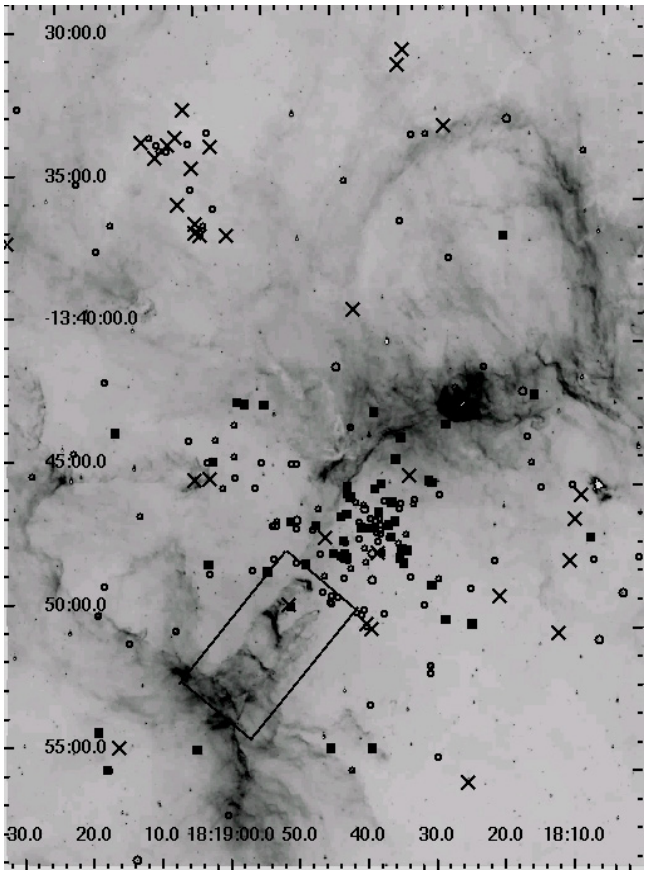

Fig. 6. IRAC image of the Eagle Nebula at 8.0 μm, centered on the cluster and covering approximately a region of $22' \times 32'$. The circles mark Class II YSOs, while the crosses mark Class I YSOs and stars consistent with both classifications. The small boxes mark massive stars. The box delimits the structures known as "elephant trunks". North is up, East is to the left.

For example, McCaughrean & Andersen (2002), using observations at high spatial resolution, showed that the trunks are stellar "nurseries", with several embedded YSOs inside them. The trunks are continuously eroded by intense incident UV flux emitted by nearby massive cluster members. As a result, some of the young sources formed inside the trunks are emerging from the photodissociation regions that delimit these structures. Due to the intense diffuse emission by the nebula, we identify only one Class I YSO emerging from the trunks, at $\alpha = 18{:}18{:}52$ and $\delta = -13{:}49{:}38$ (the cross inside the box in Fig. 6).

As shown in Fig. 6, 12 sources classified either as Class I or reddened Class II are clustered in a region in the North-West. Only one of the few Class II stars present in this region has a faint optical counterpart (with $V = 23.34^m$). Therefore, this small cluster can be associated with a denser intracluster medium and/or to more recent star-formation events, compared with the center of NGC 6611. The presence of this rich star-formation site, already suggested by Indebetouw et al. (2007), shows that the star-formation activity is still ongoing in the entire nebula, and not only in the central region.

4. Cluster members from reddening-free color indices

In Sect. 2, we discussed the different sensitivities in the four IRAC bands and how this can limit the selection of stars with

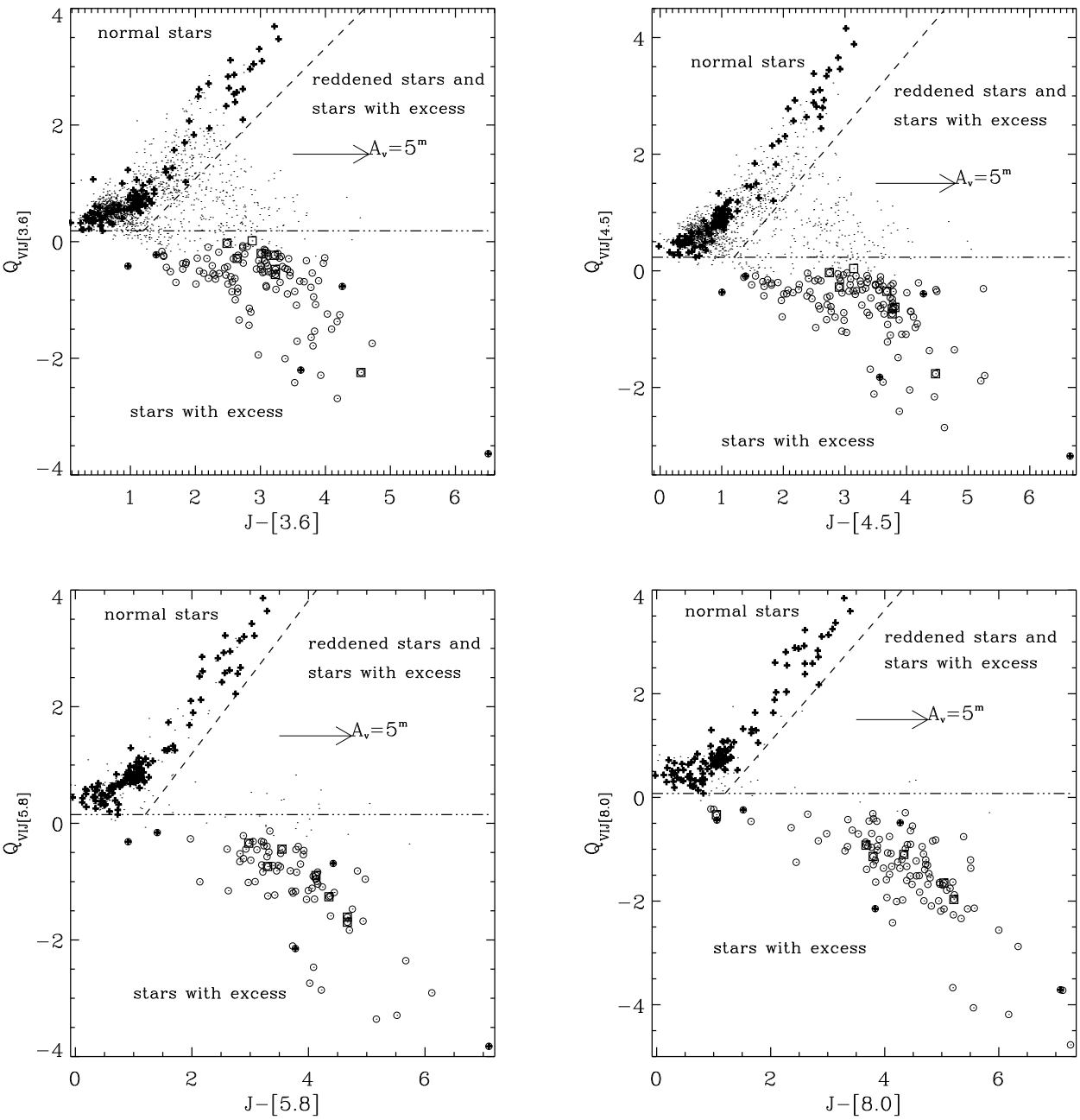

Fig. 7. Diagrams $Q_{VIJ[sp]}$ vs. the $J - [sp]$ colors for the stars in WFI FOV (points). Circles mark stars with excess in the corresponding index; the horizontal dotted-dashed lines are the lower limits for photospheric indices; the inclined dashed lines separate the locus of normal stars from that of reddened sources (or stars with small excesses). Crosses mark the optical sources used to define these limits (as explained in the text). The squares mark stars with multiple identifications.

disks by means of the IRAC color–color diagram. To partially overcome this problem, we select stars with infrared excesses also using four suitable reddening-free color indices, which we describe in detail in the following (see also GPM07 and Damiani et al. 2006).

4.1. Properties of the Q color indices

Q indices are defined to compare infrared colors with $V - I$, the latter assumed to be representative of photospheric emission:

$$Q_{VIJ[sp]} = (V - I) - (J - [sp]) \times E_{V-I}/E_{J-[sp]} \quad (1)$$

where $Q_{VIJ[sp]}$ is the index; V, I, and J are the magnitudes in the respective bands; $[sp]$ is the magnitude in a specific IRAC band; E_{V-I} and $E_{J-[sp]}$ are the reddening in the corresponding colors. E_{V-I} was inferred from the reddening law of Munari & Carraro (1996), while the extinction in IRAC bands was taken from the reddening law of Mathis 1990 (see Fig. 3). The effectiveness of this approach is that $Q_{VIJ[sp]}$ indices allow us to determine excesses in stars for which the magnitudes in all the IRAC bands are not well measured simultaneously, if V, I, and J magnitudes are known.

The identification of stars with excesses is performed using the diagrams $Q_{VIJ[sp]}$ versus $J - [sp]$ in Fig. 7. In these diagrams, the extinction applies a shift only along the x-axis, while the excess in the $[sp]$ band downward the y-axis. In this way, stars with excesses and reddened photospheres can be separated, even if a significant number of stars remain unclassified between

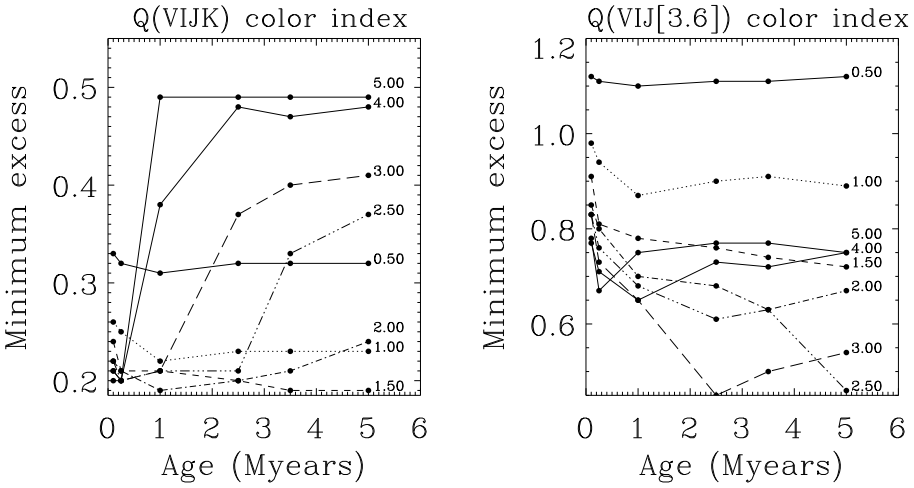

Fig. 8. Trend of the minimum excesses necessary to identify stars with excesses in K and [3.6] for the studied masses and ages values. The excesses in K are detected with the use of Q_{VIJK} index, defined in GPM07; the excess in [3.6] with $Q_{VIJ[3.6]}$.

reddened photospheres and stars with excesses. In Fig. 7, the stars with excesses are marked by circles; they are defined as the stars with the $Q_{VIJ[sp]}$ indices significantly (i.e. by more than 3 times the error in Q indices) smaller than the horizontal dotted-dashed lines, which mark the lowest limits of the photospheric $Q_{VIJ[sp]}$ indices. We define these limits as the low boundaries of the loci, in these diagrams, of the IRAC sources with optical counterparts that are clustered around the origin in the IRAC color–color plane in Fig. 3. The spatial distribution and the positions in the other color–color and color−magnitude diagrams of these stars confirm that they are field normal stars or cluster members without disk. In Fig. 7, they are marked with crosses, and it is evident that they are separated either from the stars with excesses and the reddened sources. Hereafter, we refer as *NS locus* as that of the normal stars in the diagrams in Fig. 7, to *EX locus* as that of the stars with excesses, to *UNC locus* as that of the stars consistent with both interpretations.

The minimum excesses corresponding to reliable detection of star with disk, by the use of the $Q_{VIJ[sp]}$ here and Q_{2MASS} in GPM07, is mass and age dependent. To analyze this property of Q indices, we compute these minimum excesses in [3.6] and K for stars with masses equal to 0.5, 1, 1.5, 2, 2.5, 3, 4, and 5 solar masses and with ages of 0.1, 0.5, 1, 2.5, 3.5, and 5 Myr. Their *photospheric* indices are computed with the colors predicted by the evolutionary tracks of Siess et al. (2000), using the color transformation of Kenyon & Hartmann (1995). The minimum excesses are then the excesses in [3.6] or K necessary for the Q indices to become more negative than the lower limit of photospheric colors by more than 3σ, where σ is the mean error in the Q of the sources in the WFI FOV.

Figure 8 shows the variation in the minimum excesses for one among the four indices used in GPM07 to detect excesses in K and for that used here to detect excesses in [3.6]. It is evident that for each mass and for each Q index, the minimum excesses have irregular paths with increasing age. This is due to the irregular behavior of the indices when both the involved colors become more red (or more blue), as in comparing normal stars with different effective temperatures.

Figure 8 also shows that Q_{VIJK} is more efficient in detecting excesses in stars with lower masses with respect to $Q_{VIJ[3.6]}$ index. This behavior depends on the shape of the isochrones in the Q diagrams. For example, the minimum in the 5 Myr isochrone in $Q_{VIJ[3.6]}$ of Fig. 7 occurs at ~B9 spectral type, corresponding to 2.5 $M_{\odot}$. This implies that stars of lower mass with small excesses easily fall within the *UNC* region, where we are unable to distinguish between small excesses and reddening, and therefore require stronger excesses to unambiguously ascertain the presence of disks. The corresponding minimum in the Q_{VIJK} diagram occurs at ~K4 spectral type (using the 5 Myr isochrone), implying that this index is far more efficient in detecting excesses in stars with smaller masses.

Table 2. The first column yields the $Q_{VIJ[sp]}$ indices used in this work; the second column shows the number of stars with excess detected with each $Q_{VIJ[sp]}$ index; the third column shows the total number of stars for which we compute the indices.

Q index	Number of stars with excess	Number of stars
$Q_{VIJ[3.6]}$	113	1746
$Q_{VIJ[4.5]}$	124	1474
$Q_{VIJ[5.8]}$	79	357
$Q_{VIJ[8.0]}$	104	297

A total of 174 stars with excesses are selected.

4.2. Stars with Q excesses

Table 2 indicates the total number of stars for which we compute the indices and the number of stars with excesses. These numbers may be lower limits since the criterion that we adopt to detect the stars with excesses is very conservative.

If we consider the total number of stars in our catalog with good photometry in the bands used to define the indices (third column in Table 2), we find a higher percentage of stars with excesses in the IRAC bands at longer wavelengths. This confirms that a large number of optical sources are detected in the IRAC bands at the longest wavelengths due to their nature as PMS stars, as suggested in Sect. 2.2.

Table 2 also shows a decline of the numbers of selected stars with excesses at [5.8], due to the smaller numbers of stars with good measurements in this band. This is an effect of the decrease in sensitivity with increasing wavelength. Except for 2 stars, the excesses in the three short IRAC wavelength bands are correlated. This suggests that they are related to the same physical region of the disk. This region can only be the inner rim at which disk dusts sublimate. As proposed by several authors (i.e. D'Alessio et al. 1998, 1999, 2001), this region is optically thick and emits like a blackbody at the dust sublimation temperature (between 1500 K and 2000 K). Sixteen stars have excesses only at [8.0]. This is because [8.0] can be affected by the 10 μm silicate emission feature. A Class II YSO can then exhibit excess in

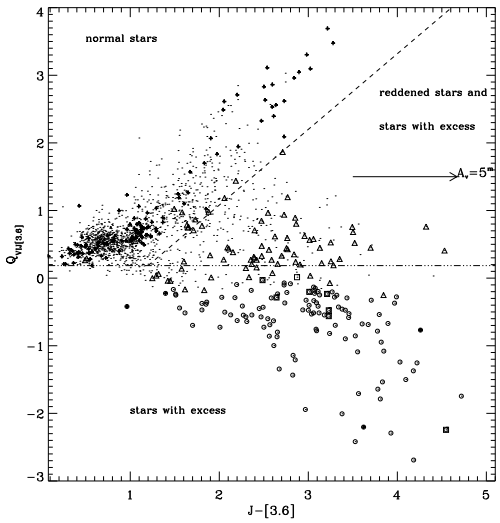

Fig. 9. Diagram of $Q_{VIJ[3.6]}$ vs. $J-[3.6]$, similar to the diagrams in Fig. 7; the stars with excesses detected in 2MASS but not in IRAC bands are marked as triangles.

[8.0] even if the inner disk is mostly evacuated, as we hypothesize for at least 4 of the 16 members of NGC 6611 with excesses detected only with $Q_{VIJ[8.0]}$ (since the other 12 are within the *UNC loci* in the other $Q_{VIJ[sp]}$ diagrams).

5. Comparison of all disk diagnostics used

Using the $Q_{VIJ[sp]}$ indices, we select 30 new stars with excesses (including 5 X-ray sources) not identified with the Q_{2MASS} indices in GPM07. Among these stars, as explained, 16 have excesses only at [8.0]; the other 14 have large errors in K band or fall inside the *UNC* loci of the Q_{2MASS} diagrams in GPM07.

Similarly, 186 stars with excesses in 2MASS bands (mostly in K) selected in GPM07, are not classified as stars with excesses by the $Q_{VIJ[sp]}$ indices. This number of stars can appear large, since usually a higher number of stars with excesses are observed at longer wavelengths. However, it must be noted that 94 of these stars have poor IRAC photometry, as reflected in the different completeness limits in the 2MASS and GLIMPSE catalogs, and therefore they are not included in the IRAC sample. All the other 92 objects are within the *UNC* loci of the diagrams in Fig. 7.

We conclude that the set of indices defined in this work is consistent with that defined in GPM07 (yielding 144 sources with at least one excess in 2MASS bands and at least one in IRAC bands). This consistency means that if Q indices detect excesses in some particular 2MASS or IRAC band, the lack of excesses in the other bands is almost always due to poor photometry or the ambiguity between excesses and reddening, as explained above. This is compatible with a scenario in which excesses in K (and H) are due to the same physical region of the disk as the excesses in the first three IRAC bands. It is important to note, however, that this consistency is true only for the Q indices, which are an efficient diagnostic for the selection of Class II YSOs with moderate disk inclination (with respect to the line of sight), because of the use of the optical and J bands. The color–color IRAC diagram is instead a peerless tool for the selection of embedded YSOs and Class II stars with highly inclined disk. Therefore, the two methods may be considered to be complementary.

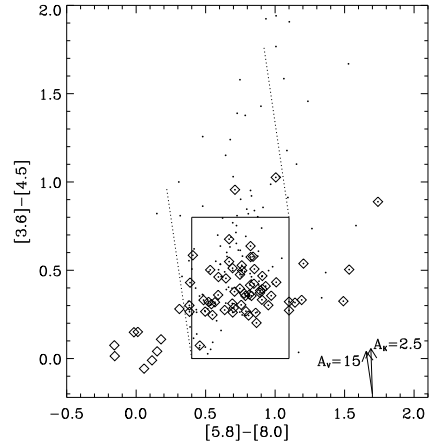

Fig. 10. IRAC color–color diagrams of the stars with disks selected with the IRAC diagram of Fig. 3 (points) and of the stars with excesses in 2MASS bands selected in GPM07 (diamonds). The Class II locus and the reddening vectors are analogous to those in Fig. 3.

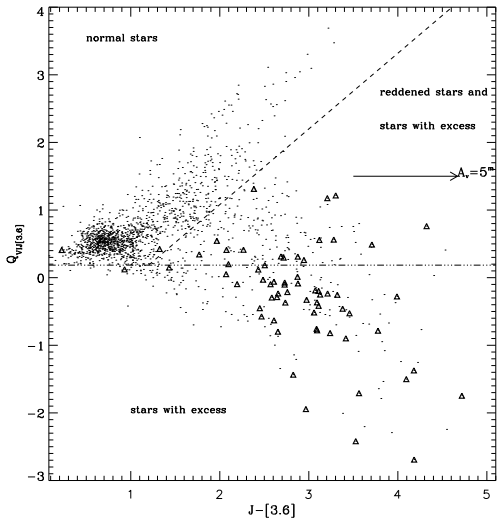

Fig. 11. Diagram $Q_{VIJ[3.6]}$ vs. $J-[3.6]$ for the stars in the WFI FOV, with overplotted the stars with excesses selected with the IRAC color–color diagram (triangles).

Figures 10 and 11 show how the excesses detected with the IRAC color–color diagram translate into those detected with Q indices, and vice versa. In Fig. 10, diamonds mark the 70 candidate stars with disks selected by GPM07 with Q_{2MASS} indices having good photometry in all IRAC bands, while dots mark the candidate stars with disk selected with the IRAC color–color diagram. Only 8 sources with excesses detected with Q_{2MASS} indices are close to the origin of the diagram (in the locus of the normal stars), while the others have red IRAC colors. The characteristics of these 8 sources will be studied by SED analysis in a future paper. Figure 11 shows the $Q_{VIJ[3.6]}$ index of candidate cluster members with disks selected with the IRAC color–color diagram (marked with triangles). As expected, almost none of these stars fall within the *NS locus*.

As a further test, Fig. 12 shows the $K-[3.6]$ versus $[3.6]-[4.5]$ diagram for the stars in ACIS FOV, with the X-ray sources and the stars with excesses in 2MASS bands selected in GPM07. All the stars with excesses in 2MASS bands have $K-[3.6] \geq 0.7^m$ and/or $[3.6]-[4.5] \geq 0.2^m$, with the exception of a couple of stars that also have both IRAC colors ~0.

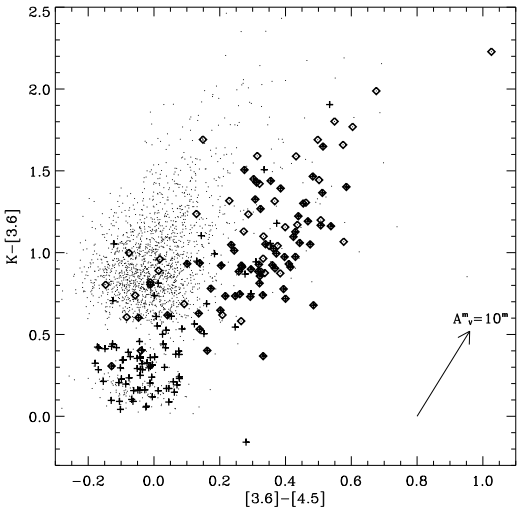

Fig. 12. Color–color diagram with K and IRAC bands for the stars in ACIS FOV (points). Diamonds are stars with excesses in 2MASS bands detected with Q_{2MASS} indices defined in GMP07, while crosses mark X-ray sources. The reddening vector, corresponding to $A_V = 10^m$, has been obtained from the extinction law of Megeath et al. (2004).

Table 3. Number of stars with excesses detected with the different diagnostics used in this paper and in GPM07.

Disk diagnostics	Numbers of stars with excesses
IRAC color–color diagram	182
Q_{2MASS} indices	330
$Q_{VIJ[sp]}$ indices	174

A total of 458 different candidate members with disk are selected.

In the diagram in Fig. 12, it is also clear that the distribution of the stars with normal colors (marked with points) shows a gap at $K - [3.6] \sim 0.5^m$, probably due to a rapid increase in the interstellar extinction at the distance of the Eagle Nebula: the foreground contaminating sources are clustered around the origin of the diagram and are clearly separated from the sample of more extincted stars, which is dominated by background sources. The gap between these two samples is populated by a large number of X-ray sources, mostly associated with the nebula.

Table 3 summarizes the number of stars with excesses selected with the diagnostics used both here and in GPM07.

6. Catalog of the candidate cluster members

Combining all the diagnostics used in this paper and in GPM07, we select a total of 1264 candidate members of NGC 6611: 790 candidate Class III members (inside the ACIS FOV) and 474 candidate Class II and Class I PMS members (inside the WFI FOV).

The catalog, available in electronic format at the CDS, comprises:

- stars IDs and coordinates;
- the magnitudes and the errors in *BVIJHK* and IRAC bands; if some value is unavailable it is set to be equal to "NAN";
- a tag (*tagx*) that is equal to 1 if the star is also an X-ray source, otherwise the tag is equal to 0;
- a tag (*tagM*) that is equal to *A*01 if the star is classified as a candidate members with disk only by its position in the IRAC color–color diagram, *A*10 if the infrared excesses are detected only by *Q* indices, and *A*11 if both diagnostics detect the emission from the disk; *B* if the star is a diskless X-ray source; *C* if it is an X-ray source with optical colors consisting with being a foreground main-sequence star (see Sect. 2).

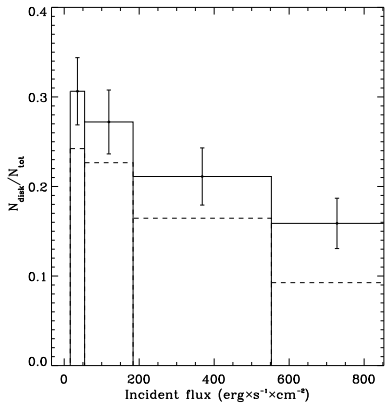

Fig. 13. Percentage of members with disks in the ACIS FOV vs. the estimated incident flux from OB members. The four values are 31% ± 4%, 27% ± 4%, 21% ± 3%, and finally 16% ± 3%, from *left to the right*.

7. Spatial variation of disks frequency

To confirm the results obtained in GPM07, we take advantage of the new list of cluster members obtained here. Inside the central 17′×17′ ACIS FOV, for which X-ray data are available, we select 790 candidate PMS members without disk, due to their X-ray emission and the presence of an optical/IR counterpart, among which 31 are likely foreground contaminants. In addition, in the same FOV we found 257 stars with NIR excesses, 54 more than in GPM07, that are candidates to have a circumstellar disk (118 are also X-ray sources).

The average disk frequency inside the ACIS FOV is 24% ± 2%, higher than the value obtained in GPM07 (19% ± 1%). Oliveira et al. (2005) measured a disk frequency of ∼58% in a small region inside the ACIS FOV. The different fraction are probably due to the different sensitivities of the two surveys. The *L* survey used in Oliveira et al. (2005) is deeper than the GLIMPSE catalog (by about 1 mag with respect to the [3.6] sources catalog). Oliveira et al. (2005) also showed that the disk frequency increases with decreasing mass of the central star, probably because the more massive the central star, the more rapid is the erosion of the circumstellar disk, as found in other star-forming regions (for example, by the study of Carpenter et al. 2006, for the Scorpius OB association). This may be the origin of the discrepancy with the Oliveira et al. (2005) results.

However, more than the absolute value of disk frequency, we are interested in its spatial variation respect to the position of massive members, which would allow us to understand whether the UV radiation emitted by the latter members can alter the disk lifetimes of nearby T-Tauri YSOs. To achieve this goal, we need only to be sure that we use a consistent criterion at different sky positions. GPM07 already used this approach, and we verify their results by using the new list of cluster members.

For every cluster member, with and without disk, we compute the incident flux emitted by 52 massive members of the cluster, of spectral class earlier than B5 (Hillenbrand et al. 1993). In this calculation, we use the projected distances from massive stars, as already explained (Sect. 1). We then compute the disk frequencies for various bins of incident flux, as shown in Fig. 13. It is evident that we confirm the main GPM07 result, i.e. that members with disks are more frequent at larger

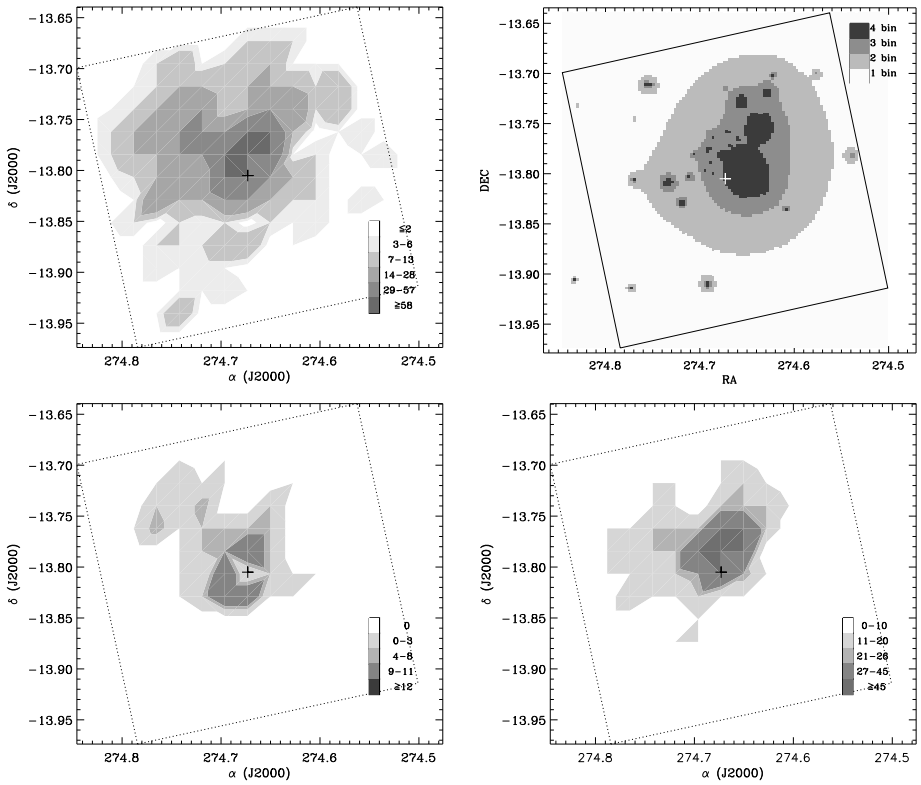

Fig. 14. *The upper left panel* shows the spatial distribution of candidate cluster members. The dotted square delimits the ACIS FOV. *The upper right panel* shows the intensity map of the radiation emitted by the massive members of the cluster. The different shades correspond to the four bins in Fig. 13. *The lower left panel* shows the spatial distribution of candidate members with disks; *the lower right panel* that of candidate members without a disk. In all the panels, the cross marks the center of the ACIS FOV.

distances from massive stars where they are irradiated by lower UV fluxes. Disk frequency, in fact, increases with decreasing incident fluxes: from 31% ± 4% in the bin with lowest flux, to 27% ± 4%, 21% ± 3%, and finally 16% ± 3% in the bin with the highest flux. In the histogram in Fig. 13, the bins size are defined in order to have the same number of diskless members in each bin. These disk frequencies are obviously more reliable than those computed in GPM07, because of our new and more complete list of cluster members. This paper, then, reinforces the result of GPM07 about the influence of massive stars on the evolution of nearby members with disks in NGC 6611.

7.1. Spatial distribution of the cluster

The panels in Fig. 14 allow us to compare directly the spatial distribution of the cluster members and the intensity of the radiation emitted by massive members. The cluster members are not equally distributed in the ACIS FOV, but an empty region exists toward the South-West. The intensity map shown in the upper right panel of Fig. 14 is more concentrated that the member density, reflecting the central concentration of massive members.

The two lower panels of Fig. 14 show the spatial distributions of disk-bearing and diskless members. We note that the latter type of stars have a more symmetrical distribution, while the former are found where the UV flux is low and their distribution also exhibits an "hole" in the center of the field, where the UV flux is higher. The region corresponding to the highest fluxes in Fig. 13 has a radius of 0.6 parsecs, the distance from massive stars at which Balog et al. (2007) found a sudden decline in disk frequency in NGC 2244.

The upper right panel of Fig. 14 also allows a more easy confrontation of our result with that of Balog et al. (2007). As explained, these authors studied the spatial variation in the disk frequency with respect to the positions of massive stars in the young cluster NGC 2244. They did not find a correlation between the two distributions, but observed a significant drop in disk frequency at distances smaller than 0.5 pc from O stars. The central regions of the intensity map in Fig. 14, corresponding to the highest fluxes in Fig. 13, has a radius equal to about 0.6 parsec, so the decrease in the disk frequency in the last bin in Fig. 13 is in agreement with the finding of Balog et al. (2007).

To estimate the extension of NGC 6611, even if it does not have a symmetrical spatial distribution, we use the 2-parameters density profile of King (1966):

$$\sigma(r) = \frac{\sigma_0}{1 + (r/r_{\rm core})^2} \quad (2)$$

where σ_0 is the central cluster density, r is the distance of stars from cluster center, and $r_{\rm core}$ is the core radius. We calculated from the observed radial density profile that $\sigma_0 = 149 \pm 8 N_{\rm stars}$ pc^{-1} and $r_{\rm core} = 1.39 \pm 0.08$ pc, in agreement with the results obtained in GPM07.

8. Summary

In this paper, we have analyzed Spitzer/IRAC data of the young open cluster NGC 6611, in the Eagle Nebula, in a large wide field of approximately $30' \times 30'$. In a previous paper, we selected members of this cluster using our published *BVIJHK* and X-ray multi band catalog. The list of cluster members that we obtained, both with and without disks, was used to verify that disk bearing cluster members are more frequent at larger distances from the massive stars.

To identify new members with disk, we have used and compared two different disk diagnostics: the IRAC color–color diagram, which uses all the IRAC bands simultaneously, and four suitable reddening-free color indices (Q indices), each defined to be able to detect the excesses in a specific IRAC band.

Using the IRAC color–color diagram, we identified 182 Young Stellar Objects (147 Class II; 13 Class I and 22 with

colors compatible with both classifications). This diagnostic is very efficient in selecting primarily embedded young sources, but can be used only for stars with high quality photometric data in all IRAC bands. We discuss how significantly this affects the selection of faint YSOs. With the use of Q indices, we partially overcome this problem, since they allow us to select stars with excesses in each individual IRAC band; with this diagnostic, we selected 174 YSOs with excesses in IRAC bands. Among them, 66 stars could not be detected with the IRAC color–color plane, since they were not reliably detected in all the IRAC bands.

Combining the outcome of both diagnostics, we identify 146 new cluster members with disks with respect to our previous work, which was based on 2MASS photometry alone (116 from the IRAC color–color diagram and 30 from Q indices). In the end, our combined catalog includes a total of 474 candidate Pre-Main Sequence members with disks and 790 without disks (the latter only in the central $17' \times 17'$ field, where we found 118 X-ray sources with disks).

Comparing all of the Q indices defined with 2MASS and IRAC bands (with the exception of [8.0] band), we claim that they are all sensitive to the emission from the same physical region of the disk, namely the inner rim at the dusts sublimation radius. These indices will be efficiently used, then, to select Class II stars that are not largely embedded (i.e. for which it is possible to detect the photospheric emission) and whose inner disk is not evacuated. The embedded YSOs associated with the cluster can be selected only by the IRAC color–color diagram, and not with the Q indices.

We discuss evidence suggesting that star-formation activity is ongoing in the outer region of the Eagle Nebula, and not only in the center of NGC 6611 as shown by previous works. For example, the diagnostic based on the IRAC color–color diagram allows us to identify a probable new star-formation site, rich in Class I and embedded Class II objects, toward the North with respect to the center of the cluster.

In the central $17' \times 17'$ field, we have measured an average disk fraction equal to $24\% \pm 2\%$. In this field, the disk frequency also has a strong dependence on the incident radiation emitted by massive members, varying from $31\% \pm 4\%$ to $16\% \pm 3\%$ across the complete range of values of incident flux. This is an evidence of the influence of massive stars radiation on the evolution of circumstellar disks and star-formation process, as already shown in GPM07.

Acknowledgements. We thank the anonymous referee for comments and suggestions that allowed us to improve our manuscript. We acknowledge financial support from the contract PRIN-INAF. This publication makes use of Spitzer's GLIMPSE survey data.

References

Adams, F. C., Proszkow, E. M., Fatuzzo, M., & Myers, P. C. 2006, ApJ, 641, 504
Allen, L. E., Calvet, N., D'Alessio, P., et al. 2004, ApJS, 154, 363
Balog, Z., Muzerolle, J., Rieke, G. H., et al. 2007, ApJ, 660, 1532
Benjamin, R. A., Churchwell, E., Babler, B. L., et al. 2003, PASP, 115, 953
Calvet, N., Hartmann, L., Kenyon, S. J., & Whitney, B. A. 1994, ApJ, 434, 330
Carpenter, J. M., Mamajek, E. E., Hillenbrand, L. A., & Meyer, M. R. 2006, ApJ, 651, L49
D'Alessio, P., Canto, J., Calvet, N., & Lizano, S. 1998, ApJ, 500, 411
D'Alessio, P., Calvet, N., Hartmann, L., Lizano, S., & Cantó, J. 1999, ApJ, 527, 893
D'Alessio, P., Calvet, N., & Hartmann, L. 2001, ApJ, 553, 321
Damiani, F., Maggio, A., Micela, G., & Sciortino, S. 1997, ApJ, 483, 350
Damiani, F., Prisinzano, L., Micela, G., & Sciortino, S. 2006, A&A, 459, 477
Eisner, J. A., & Carpenter, J. M. 2006, ApJ, 641, 1162
Fatuzzo, M., & Adams, F. C. 2008, ApJ, 675, 1361
Fazio, G. G., Hora, J. L., & Allen, L. E. 2004, ApJS, 154, 10
Flaherty, K. M., Pipher, J. L., Megeath, S. T., et al. 2007, ArXiv Astrophysics e-prints
Guarcello, M. G., Prisinzano, L., Micela, G., et al. 2007, A&A, 462, 245
Gutermuth, R. A., Myers, P. C., Megeath, S. T., et al. 2008, ApJ, 674, 336
Gvaramadze, V. V., & Bomans, D. J. 2008, ArXiv e-prints, 809
Haisch, Jr., K. E., Lada, E. A., & Lada, C. J. 2001, ApJ, 553, L153
Hillenbrand, L. A., Massey, P., Strom, S. E., & Merrill, K. M. 1993, AJ, 106, 1906
Indebetouw, R., Robitaille, T. R., Whitney, B. A., et al. 2007, ArXiv e-prints, 707
Kenyon, S. J., & Hartmann, L. 1995, ApJS, 101, 117
Kenyon, S. J., Calvet, N., & Hartmann, L. 1993, ApJ, 414, 676
King, I. R. 1966, AJ, 71, 64
Linsky, J. L., Gagné, M., Mytyk, A., McCaughrean, M., & Andersen, M. 2007, ApJ, 654, 347
Mathis, J. S. 1990, ARA&A, 28, 37
McCaughrean, M. J., & Andersen, M. 2002, A&A, 389, 513
Megeath, S. T., Allen, L. E., Gutermuth, R. A., et al. 2004, ApJS, 154, 367
Mendoza V., E. E. 1966, ApJ, 143, 1010
Mendoza V., E. E. 1968, ApJ, 151, 977
Meyer, M. R., Calvet, N., & Hillenbrand, L. A. 1997, AJ, 114, 288
Munari, U., & Carraro, G. 1996, A&A, 314, 108
Oliveira, J. M., Jeffries, R. D., van Loon, J. T., Littlefair, S. P., & Naylor, T. 2005, MNRAS, 358, L21
Prisinzano, L., Micela, G., Flaccomio, E., et al. 2008, ApJ, 677, 401
Siess, L., Dufour, E., & Forestini, M. 2000, A&A, 358, 593
Störzer, H., & Hollenbach, D. 1999, ApJ, 515, 669